SIMPLIFIED MODELLING OF EXPLOSION PROPAGATION BY DUST LIFTING IN COAL MINES

Skjold, T.[‡ 1,2], Eckhoff, R.K.[2], Arntzen, B.J.[2,1], Lebecki, K.[3], Dyduch, Z.[3], Klemens, R.[4], & Zydak, P.[4]

[1] *GexCon AS, Bergen, Norway*
[2] *University of Bergen, Department of Physics and Technology, Bergen, Norway*
[3] *Central Mining Institute, Katowice, Poland*
[4] *Warsaw University of Technology, Institute of Heat Engineering, Warsaw, Poland*

ABSTRACT

Dispersion of accumulated layers of combustible dust by turbulent flow or shock waves ahead of the propagating flame may sustain explosion propagation in coal mine galleries and other industrial facilities. The mechanisms involved in transforming dust layers into dust suspensions are rather complex, and detailed numerical modelling of this process is therefore practically impossible, at least on industrial scales. In the computational fluid dynamics code DESC (Dust Explosion Simulation Code), a simplified empirical relation describes the dust-lifting phenomenon. The relation originates from experimental work in a laboratory-scale shock tube, and a small wind tunnel, at Warsaw University of Technology. The present paper describes the modelling of dust lifting in the current version of DESC, and illustrates the performance of the code by simulating some large-scale dust explosion experiments conducted in a 100-m surface gallery at the Experimental Mine Barbara in Katowice, Poland. Although there are significant uncertainties associated with this type of calculations, the results suggest that a simplified approach to dust lifting may become a useful tool for risk assessments in the future.

INTRODUCTION

Dust and gas explosions represent a significant hazard in underground coal mines. The risk to miners can be significantly reduced by various preventive and mitigating measures, such as improved ventilation, detection systems for flammable gas, rock dusting, passive and active barriers, and more automated mining techniques (i.e. less personnel in the mines) [1-3]. However, optimal design of explosion mitigation systems is often hampered by both limited capabilities in predicting the course of large-scale explosions and a general lack of knowledge about the physical phenomena involved in explosion accidents.

Faraday & Lyell [4] for the first time documented the significant role played by the coal dust in major coal mine explosions [5]. The sequence of events leading up to such accidents often starts out with the formation of a flammable gaseous mixture, usually methane/air (or 'fire-damp'). If an ignition source is present, turbulent flow or shock waves generated by a primary gas explosion may disperse accumulated layers of coal dust, and a secondary dust explosion may propagate through the mine gallery [6,7]. The dust explosion may then escalate further through mechanisms such as continuous dispersion of accumulated coal dust ahead of the flame front, flame acceleration by repeated obstacles (e.g. pillars in mine galleries), pressure piling and jet ignition in connected enclosures, and in extreme cases even transition to detonation [8].

Accidental dust explosions involve compressible transient turbulent reacting multiphase flow in complex geometries. Hence, computational fluid dynamics (CFD) is required for solving the relevant differential equations, describing conservation of mass, momentum, and energy. However, inherent limitations in the available computational recourses limit the achievable spatial and temporal resolution of such calculations, and it is necessary to adopt various simplifying assumptions or subgrid

[‡] Corresponding author; *tel.:* +47 55 57 40 26; *e-mail:* trygve@gexcon.com

models in the calculations. Nevertheless, the goal of the DESC project was to develop a simulation tool based on CFD that could predict the potential consequences of industrial dust explosions [9]. The European Commission supported the project, and GexCon released the first version of the resulting CFD code, DESC 1.0, in June 2006 [10].

As part of the DESC project, a research group at Warsaw University of Technology (WUT) investigated the mechanism of dust lifting both theoretically and experimentally. The theoretical investigations suggested that detailed modelling of dust lifting should account not only for the Magnus and Saffman forces, but also for particle collisions [11]. However, it is currently not feasible to model the detailed mechanisms of these interactions on a scale suitable for industrial applications, and an empirical approach was therefore adopted for the first versions of the DESC code. From experiments in a 5-6 m experimental stand that could be operated as either a shock tube or a wind tunnel, it was possible to deduce an empirical relation where dust lifting is described as ejection of dust from a horizontal layer [12, 13]. The present paper investigates the general applicability of this simple empirical correlation for dust lifting by simulating some large-scale explosion scenarios where flame propagation by dust lifting played an important role. Simulation results obtained with the CFD-code DESC are compared with results obtained in experiments performed by Central Mining Institute (CMI) in the 100-meter surface gallery at Experimental Mine Barbara [14-16].

MODELLING IN DESC

DESC has many features in common with the CFD code FLACS (FLame ACceleration Simulator) for gas explosions [10]. Both FLACS and DESC are finite volume CFD codes where transport equations for mass, momentum, enthalpy, fuel, mixture fraction, turbulent kinetic energy k, and rate of dissipation of turbulent kinetic energy ε, are solved on a 3-dimentional structured Cartesian grid. A porosity concept maps all solid objects to the computational grid: each grid cell is assigned one volume porosity and six surface porosities. Sub-grid models describe phenomena that are not resolved on the computational grid, such as initial flame propagation and turbulence production by flow past small-scale objects. Users define explosion scenarios (i.e. geometry, grid, initial conditions, boundary conditions, time/position of ignition, monitor points, pressure relief panels, output parameters, etc.) in the pre-processor CASD (Computer Aided Scenario Design), and view/export results from the simulations (i.e. scalar time plots, scalar line plots, 2D cut plane plots, volume plots, etc.) in the post-processor Flowvis. The most important numerical schemes include the SIMPLE algorithm for compressible flow [17], first order backward Euler time differencing scheme, second order upstream and central differencing scheme for convective fluxes, second order central differencing scheme for diffusive fluxes, and conjugant gradient solvers. A standard k-ε model describes turbulent flow [18], with additional source terms for turbulence production by velocity gradients. The combustion models in FLACS and DESC are also similar: the reaction zone is defined by a flame thickening model [19], and the burning velocity is taken from empirical data [10] and correlations originating from experimental work on gaseous fuels [20,21].

Particle-laden flows are treated as equilibrium mixtures [22], i.e. the dispersed particles are assumed to be in dynamic and thermal equilibrium with the gaseous phase. This corresponds to an Eulerian approach in the limiting case when the Stokes number approaches zero [23]. Since there is no slip velocity between the continuous and dispersed phases, it is not possible to model phenomena such as dust settling, or flow separation in bends and cyclones. Dispersion of accumulated dust layers follows an empirical correlation obtained through experiments on dust lifting by turbulent flow or shock waves at WUT [12,13,24]. In the experiments, uniform dust layers with initial thickness equal to 0.1, 0.4 or 0.8 mm were prepared on a 1.5 m metal insert by a specially designed pneumatic system, before the insert was placed inside a 5-6 m long shock tube / wind tunnel with internal cross section 0.072 m × 0.112 m. After passing of a shock wave, or after the onset of turbulent flow, a technique based on attenuation of laser beams measured the increase in dust concentration at various heights above the layer. From these experiments, it was possible to deduce an empirical correlation that describes dust lifting as release of dust from a horizontal surface. The following relation gives the mass flux of dust as an injection velocity v_z in m s^{-1}, assuming a dust concentration c_d equal to 1 kg m^{-3}:

$$v_z = 0.004\, h_l^{0.216}\, u^{1.742}\, d_p^{-0.053}\, \rho_p^{-0.160}\, A_p^{0.957} \qquad (1.1)$$

where h_l is layer thickness in millimetres, u is flow velocity above the layer in m s^{-1}, d_p is a characteristic particle size in μm, ρ_p is particle density in kg m^{-3}, and A_p is a dimensionless empirical constant. For a given mass of dust m_d, evenly distributed over a rectangular surface with length L and width W, the surface density σ_l of the dust layer is:

$$\sigma_l = \frac{m_d}{LW} \tag{1.2}$$

As dust is raised into suspension, the thickness of the static dust layer decreases. Hence, it is most convenient to specify a dust layer by its position, size, initial surface density, and bulk density:

$$\rho_b = \frac{m_d}{LW}\frac{1}{h_l} = \frac{\sigma_l}{h_l} \tag{1.3}$$

Figure 1 shows the results from some selected dust concentration measurements from the experiments at WUT where airflow generated by a centrifugal fan dispersed coal dust layers from the bottom of the duct [24]. The flow velocity at the channel axis was about 29 m s^{-1}, and the laser system was located 1.115 m downstream of the beginning of the dust layer. The figure shows that the thicker dust layers produce higher dust concentrations in the upper part of the duct, for a longer period, compared to the thinner layers.

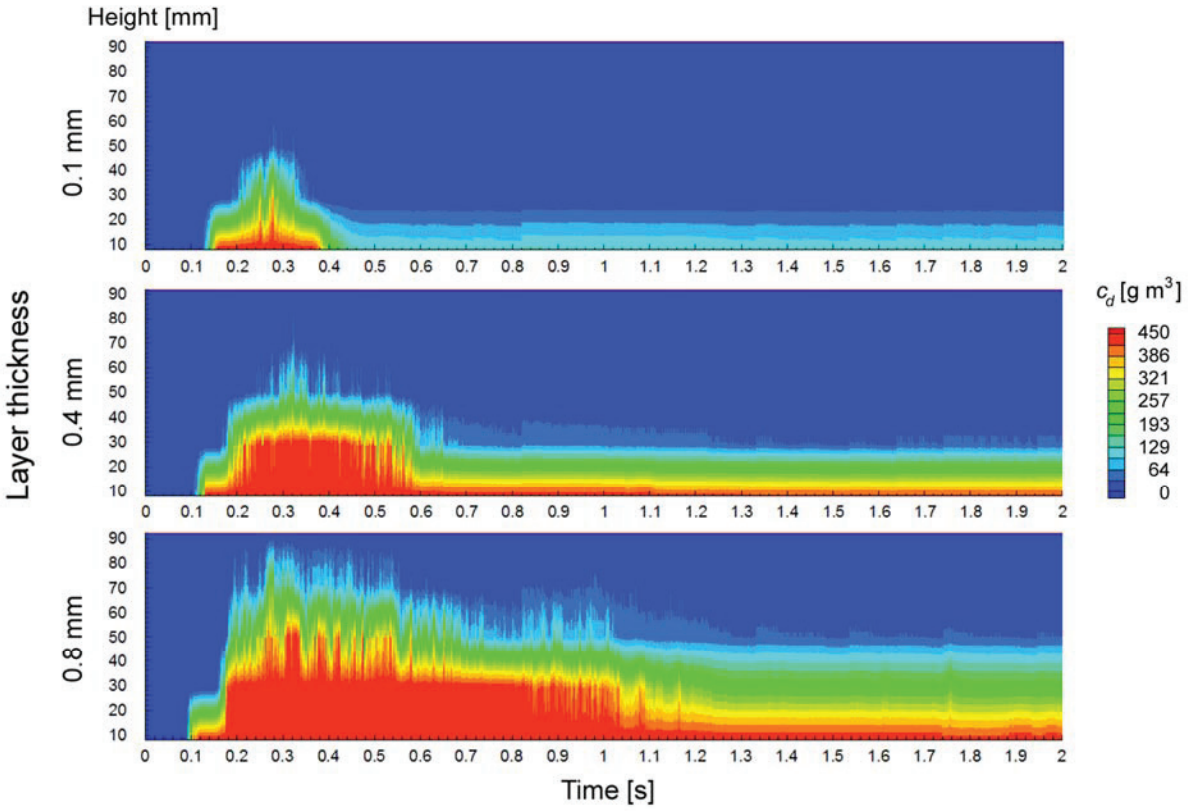

Fig. 1 *Measured coal dust concentrations as function of time and height above the layer for three different layer thicknesses (Figures from [24] – Report IV, Annex 2).*

Figs. 2 and 3 show the results from DESC simulations of the process illustrated in Fig. 1, for four different grid configurations:

A. 14 mm cubical grid cells, completely ongrid
B. 14 mm cubical grid cells, a 1 mm porous object resolved by refined grid cells above the layer
C. 14 mm cubical grid cells, a 1 mm porous object creates volume porosities in cells above the layer
D. 7 mm cubical grid cells, a 1 mm porous object creates volume porosities in cells above the layer

In the simulations, the parameters in Eq. (1.1) are set to: ρ_p = 1340 kg m^{-3}, ρ_b = 600 kg m^{-3}, d_p = 18 μm and A_p= 1.2. From comparing Figs. 1 and 2, it is evident that the simulated dust dispersion process is not raising the dust cloud as high up in the channel as measured in the experiments. This is primarily

due to an inherent limitation resulting from the equilibrium mixture assumption mentioned earlier. Enforcing 'no slip' between the particle and fluid phases inevitably means that the vertical injection velocity in Eq. (1.1) in reality becomes a diffusive mass flux (since the injected dust concentration is fixed). The discrepancies between the results obtained by using various grid configurations (A-D) are primarily due to the presence of volume porosities in the grid cells immediately above the layer in some of the simulations. Since the porous object in case B is resolved on the grid, the results become practically identical to the ongrid case (A). However, when the porous object becomes 'distributed' throughout the grid cells immediately above the layer (cases C and D), the horizontal velocity through these cells is somewhat reduced due to the added flow restriction, resulting in a prolonged duration of the injection process (possibly in better agreement with the experiments illustrated in Fig. 1). The presence of volume porosities also promotes production of turbulent kinetic energy (due to subgrid models), and thereby enhanced mixing. Hence, it is in principle possible to manipulate the mass flux from the layer by introducing off-grid porous objects above the layer. The finer grid in case D results in sharper gradients and increased volume porosities in the cells immediately above the layer, and this enhances transport of dust to the upper parts of the duct.

It should however be noted that the relatively high degree of spatial resolution used in the simulations described above cannot be achieved when modelling dust explosions in coal mines or industrial powder handling plants. Grid cells in such situations will typically be on the order 0.1 to 1 m, and dust lifting significantly beyond the first layer of grid cells will have to rely on convection (turbulent mixing).

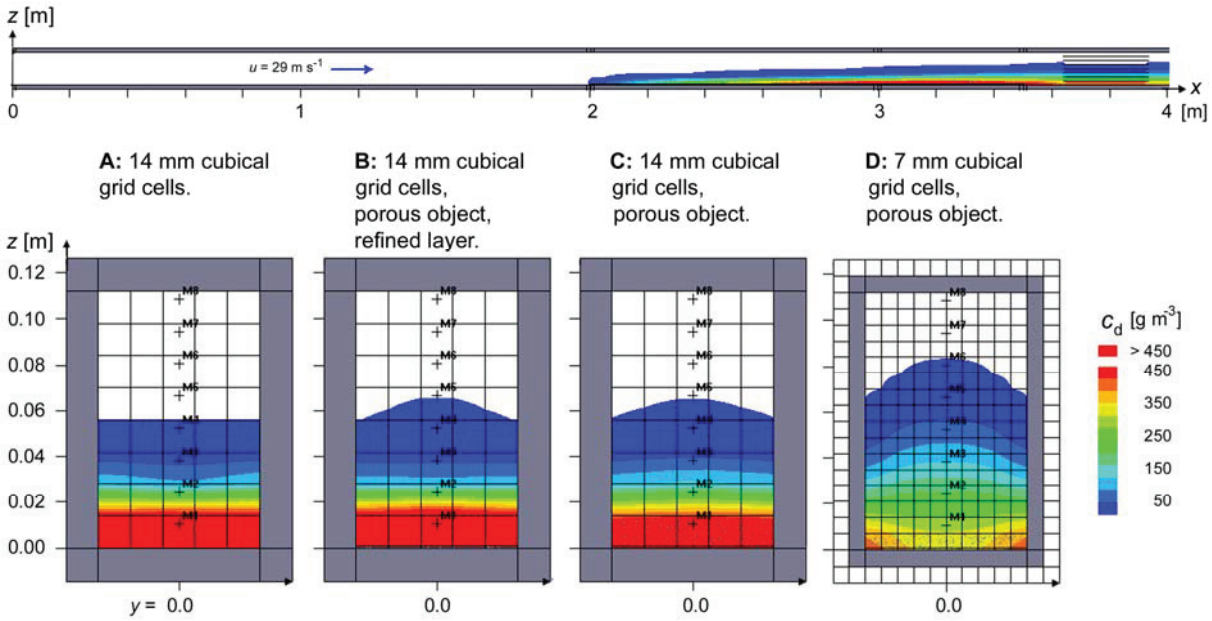

Fig. 2 *Simulated coal dust concentrations in vertical cross-sections of the wind tunnel from WUT for four different grid cell and geometry configurations (A-D).*

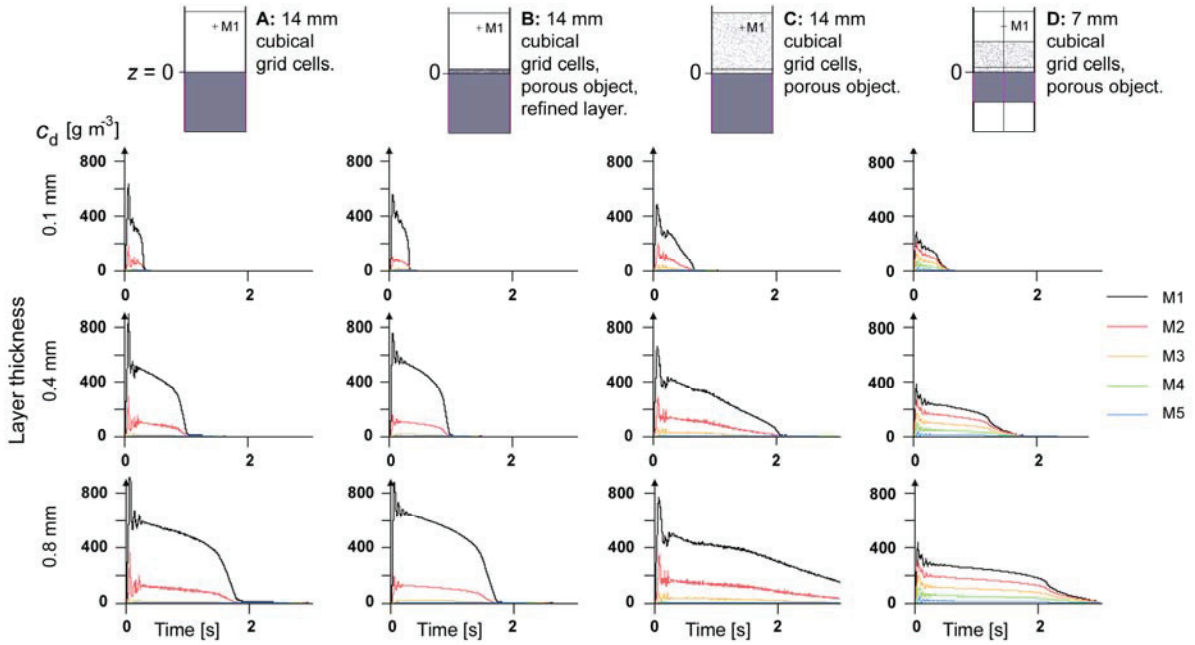

Fig. 3 *Simulated coal dust concentrations for the four configurations illustrated in Fig. 2 (the monitor points M1-M5 are shown in Fig. 2).*

LARGE-SCALE EXPERIMENTS

Experiments performed in the 100 m surface gallery at Experimental Mine Barbara in 1990 [14-16] are used here as examples of dust lifting scenarios at significantly larger scale than the experiments behind the empirical model in DESC. Contrary to most large-scale dust explosion experiments, dust concentrations were measured in the centre of the gallery, 1 m above the ground. Fig. 4 illustrates the gallery and experimental results from the three tests investigated here, and Table 1 summarizes the experimental conditions in the tests.

Table 1: *Experimental conditions for the three tests in the 100 m surface gallery (Fig. 4); the coordinates from 0 to 100 m start in the closed end of the gallery.*

Test no.	ST3332	ST3333 & ST3334
Initial fuel distribution	0.0 – 3.5 m 9.5 % CH_4 in air 3.5 – 8.5 m 3 kg maize dust on floor 8.5 – 13.5 m no dust 13.5 – 18.5 m 3 kg maize dust on floor 18.5 – 23.5 m no dust 23.5 – 28.5 m 3 kg maize dust on floor 28.5 – 33.5 m no dust 33.5 – 38.5 m 3 kg maize dust on floor 38.5 – 43.5 m no dust 43.5 – 48.5 m 3 kg maize dust on floor 48.5 – 53.5 m no dust 53.5 – 58.5 m 3 kg maize dust on floor 58.5 – 63.5 m no dust 63.5 – 68.5 m 3 kg maize dust on floor 68.5 – 100 m no dust	0.0 – 3.5 m 9.5 % CH_4 in air 3.5 – 23.5 m 6 kg maize dust on shelves 23.5 – 43.5 m no dust 43.5 – 63.5 m 6 kg maize dust on shelves 63.5 – 100 m no dust
Primary explosion	10 m^3 CH_4 in air – 9.5 %	10 m^3 CH_4 in air – 9.5 %
Dust	Maize dust – unknown particle size distribution and K_{St} value	
Flame range	50 – 60 m	40 – 50 m (ST3333) & 60 – 70 m (ST3334)

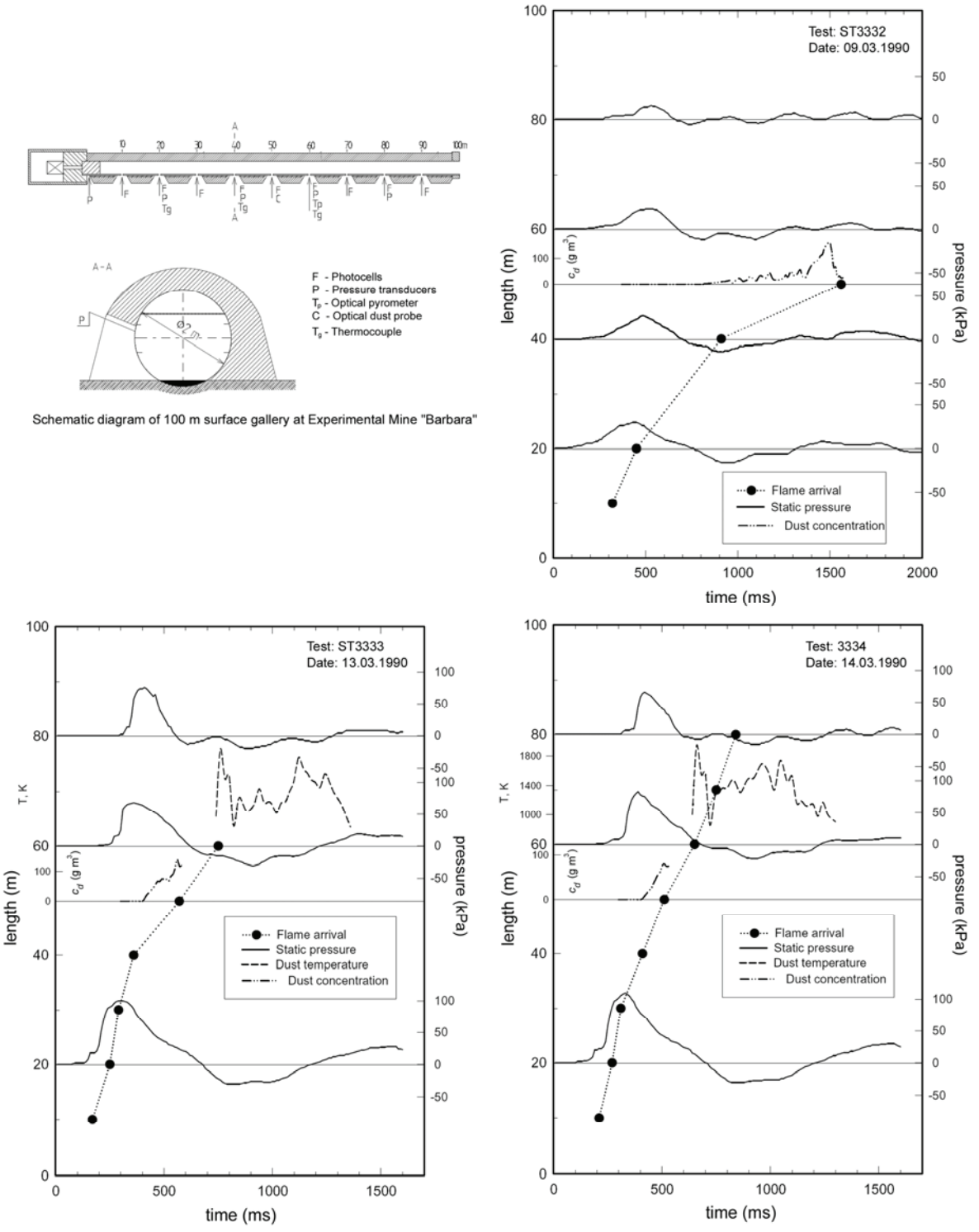

Fig. 4 *Schematic diagram of the 100 m surface gallery, and wave diagrams from the three tests investigated in this paper (ST3333 and ST3334 are repeated tests).*

There are significant differences between the results obtained in the three tests in Fig. 4. Although all tests were initiated with a primary explosion in a 10 m^3 stoichiometric methane-air mixture, the first peak in the pressure pulse from the test with dust layers on the floor (ST3332) is only about 0.3 barg, i.e. significantly lower than the about 1 bar overpressures observed in the two tests with dust layers on shelves (ST3333 and ST3334). The flame also propagated more slowly in the test with floor layers, compared to the other two tests where the first 40 meters of flame propagation were quite similar.

Beyond 40 meters, the flames slowed down quite rapidly and stopped after 60 meters in test ST3333, but continued at relatively constant speed up to 80 meters in test ST3334. Common to all three tests is a distinct increase in the measured dust concentration, to about 100 g m^{-3}, immediately prior to flame arrival in the middle of the gallery (length = 50 m).

SIMULATIONS

There are only two fundamentally different explosion scenarios to simulate with DESC, since two of the tests in Table 1 were conducted from the same initial conditions. However, since detailed knowledge about the dust samples used in the tests were not available, several additional simulations were included to cover a reasonable variation in both the dispersability of the dust layers and the reactivity of the dust clouds. The simulations included two values of the empirical dust lifting constant A_p in Eq. (1.1), 0.6 and 1.2, and the other material parameters were set to: ρ_p = 1180 kg m^{-3}, ρ_b = 600 kg m^{-3}, and d_p = 15 μm. The maize dust were assumed to have properties similar to maize starch with K_{St} equal to 150 bar m s^{-1}, but simulations with 25 % reduction and 25 % enhancement of the reactivity (more precisely: the estimated laminar burning velocity S_L), were also included. Unfortunately, it was not possible to define two different types of fuel (i.e. methane and combustible dust) in the same DESC simulation, and in all simulations involving dust lifting the 10 m^3 quiescent methane-air mixture was therefore replaced with a dust cloud of the same initial size (concentration 350 g m^{-3}). For reference, two additional simulations without any dust layers were also included: a FLACS simulation with an initial 10 m^3 quiescent stoichiometric methane-air mixture in the closed end of the gallery, and a DESC simulation with an initial 10 m^3 turbulent 350 g m^{-3} dust cloud in the same position. Hence, the total number of simulations was 14. The computational grid consisted of 0.20-meter cubical grid cells throughout the gallery, and stretched towards the boundary 10 meters beyond the open end. Figs. 5 and 6 summarize the results obtained in the two simulations without dust layers, and the four simulations with standard dust cloud reactivity, and Fig. 7 illustrates the estimated flame lengths as function of time for the 13 DESC simulations.

The simulation results summarized in Fig. 5 cover the following six explosion scenarios:

1. Only primary explosion in 10 m^3 stoichiometric methane/air mixture.
2. Only primary explosion in 10 m^3 dust/air mixture with concentration 350 g m^{-3}.
3. Primary explosion in 10 m^3 dust/air mixture (350 g m^{-3}) and dust layers on floor: A_p = 0.6
4. Primary explosion in 10 m^3 dust/air mixture (350 g m^{-3}) and dust layers on floor: A_p = 1.2
5. Primary explosion in 10 m^3 dust/air mixture (350 g m^{-3}) and dust layers on shelves: A_p = 0.6
6. Primary explosion in 10 m^3 dust/air mixture (350 g m^{-3}) and dust layers on shelves: A_p = 1.2

From the reference simulations without dust layers (Figs. 5 and 6), it is evident that the simulated methane explosion (1) is significantly more violent than the dust explosion (2). This is primarily a result of delayed start-up of the dust explosion on the relatively coarse grid, where the effect of turbulence is not properly account for by the subgrid model that governs the initial phase of flame propagation in DESC [25], and this effect is reinforced by the higher reactivity of the methane/air mixture. It is also worth noticing that the pressure pulses from the pure methane simulation are quite similar to the experimental results from the two tests with dust layers on the floor. However, apart from the somewhat reduced amplitude, and a 0.4-0.5 s delay for the dust explosion, the pressure pulses from the two primary explosions are quite similar in shape. The main characteristics of the pressure pulses remain practically unchanged when dust lifting is included in the simulations (in Fig. 6 the pulse from scenario 1 is included as reference in the plots for scenarios 3-6).

Figs. 5 and 7 illustrate that the flames in scenarios 3-6 are able to propagate significantly beyond the flames from the primary explosions due to dust lifting from the layers, and that the simulated dust concentrations in the centre of the gallery increase to values similar to those measured (Fig. 4). Fig. 7 shows that both the dispersability of the dust layers and the reactivity of the dust clouds have significant effect on flame propagation.

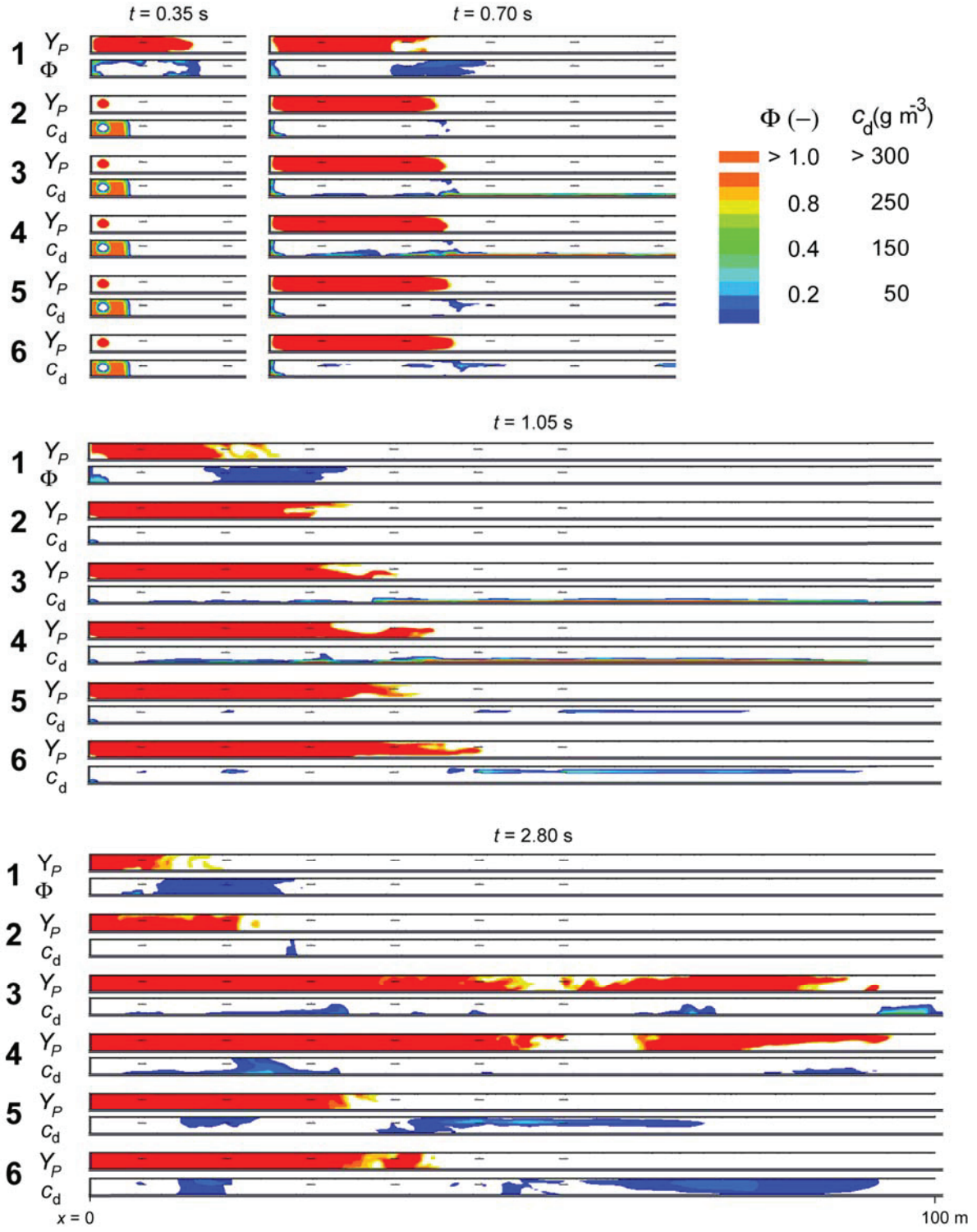

Fig. 5 *Simulated flame propagation illustrated by mass fraction of combustion products (Y_P), and corresponding concentrations (dust concentration c_d, or equivalence ratio Φ for methane) at various time steps in the two simulations without dust layers and the four simulations with standard reactivity.*

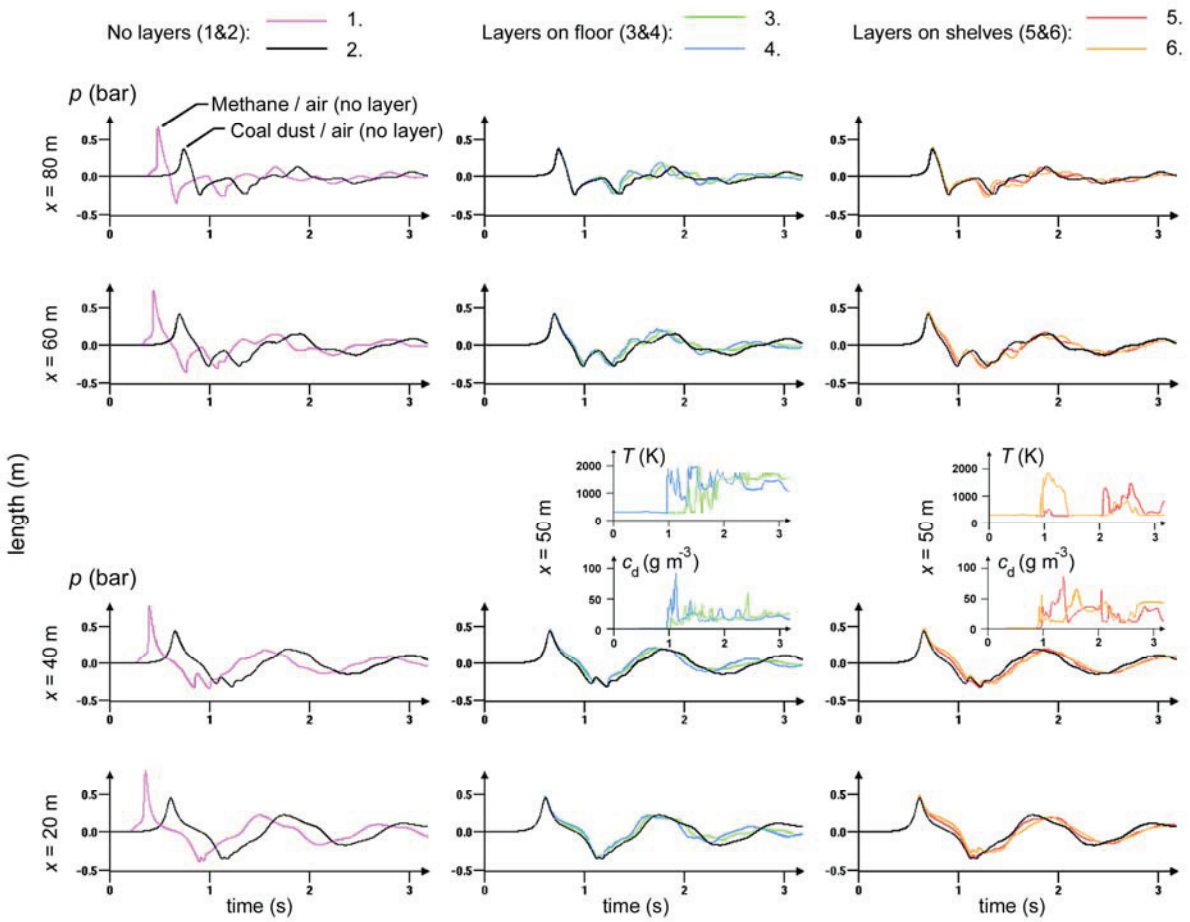

Fig. 6 *Simulated pressure-time plots (at 20, 40, 60, and 80 m), dust concentrations (at 50 m), and temperatures (at 50 m), in the two simulations without dust layers (only methane-air or dust-air clouds) and the four simulations with standard reactivity.*

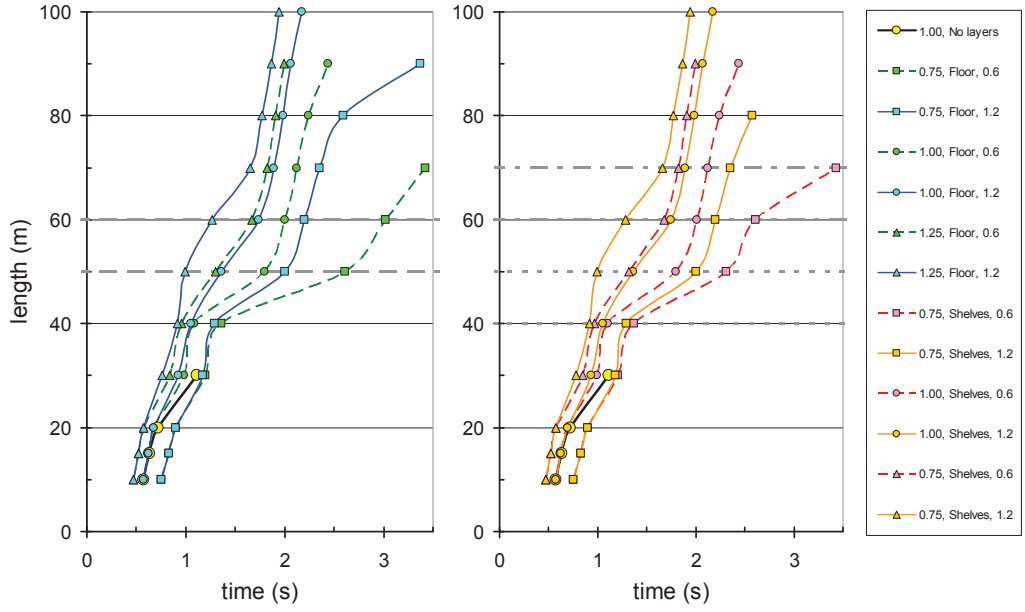

Figure 7 *Length of flame propagation as function of time for the 13 DESC simulations. The legend indicates the reactivity of the dust clouds (0.75, 1.0 or 1.25 times the estimated laminar burning velocity), the configuration of dust layers (no layer, layers on floor, or layers on shelves; see Table 1), and dispersability of the dust layer (the value of A_p set equal to either 0.6 or 1.2).*

DISCUSSION

The simulated pressure pulses in Fig. 6 indicate that the primary explosion dominates the pressure development in the gallery, and the effect of additional combustion of dispersed dust is therefore difficult to isolate when comparing measured and simulated pressures. Although there are significant uncertainties associated with this type of simulations, it is not straightforward to explain why the primary explosion in the experiment with dust layers on the floor produced significantly weaker pressure pulses compared to the two tests with dust layers on the shelves. It is possible that the initial blast was able to disperse a higher fraction of dust from the shelves, compared to the floor, but a leaner initial methane-air mixture in test ST3332, compared to tests ST3333 and ST3334, could also be a possible explanation. Future validation work should focus on experiments where the primarily explosion plays a less important role in the overall pressure development, for instance galleries with a much larger L/D ratio [26].

Although the simulated flames in Fig. 5 propagate a longer distance than the measured flames in Fig. 4, and there is significant spread in the simulated results depending on the reactivity and dispersability of the dust, the results on flame propagation seem to agree quite well with experimental data for dust layers on the shelves. Because there is no dust settling in the simulations, and not all of the dust would contribute in the experiments, it seems quite reasonable that the simulated flame propagation is more extensive than that measured. The flames in both experiments and simulations show a tendency to slow down after the first 30-40 meters of flame propagation, and the simulations illustrate that the point of onset of this process depends strongly on both the reactivity of the dust cloud and the dispersability of the dust layer.

It is generally not straightforward to simulate dust explosion experiments described in literature because of limited exposure of technical details. The modelling of large-scale explosions is in itself a challenging task, and it is often difficult to properly reproduce the initial and boundary conditions from the experiment: transient flow conditions during dust dispersion, strong ignition sources, dust layer properties (thickness, uniformity, bulk density), geometrical details, etc. In most cases, there are also significant uncertainties associated with relevant properties of the dust, such as particle size distribution, humidity, volatile content, reactivity, heat of formation, heat capacity, chemical composition, etc. However, since large-scale dust explosion experiments are very expensive, and hence difficult to realize, it seems worthwhile indeed to try to utilize such data, keeping in mind their inherent limitations.

The DESC simulations presented in this paper illustrate some of the dilemmas associated with developing CFD codes for consequence assessments in the process industry. In principle, more advanced modelling, finer grid resolution, alternative grid systems, etc. can always bring the simulation results closer to reality. However, there is usually a trade off between approaching physically correct models, and acceptable computational cost. No doubt, more advanced modelling of multiphase flows in DESC would improve the simulation results illustrated in Fig. 2, and most likely reduce the length of flame propagation in Fig. 7 due to dust settling. However, solving the additional equations required for improved two-phase modelling would increase both calculation time and memory consumption, and simulated dust settling based on inaccurate assumptions concerning particle size or density could under-predict the length of flame propagation. Hence, the development and maintenance of this type of software involves challenging validation work, a continuous quest for improved physical models and numerical schemes, with a constant awareness of the implications for process safety.

CONCLUSIONS

Although practical consequence assessments concerning large-scale dust explosions in coal mines or other industrial facilities will always be associated with significant uncertainties, the use of CFD offers an approach that can provide both improved safety and increased understanding of the physical phenomena involved in such accidents. Further validation of the approach presented here is definitely required, but the results nevertheless demonstrate that simplified modelling of dust lifting may be beneficial for safety engineering applications.

ACKNOWLEDGEMENTS

The authors gratefully acknowledge all contributions from partners in the DESC project, and the financial support from the European Commission.

REFERENCES

1. Sapko, M.J., Weiss, E.S., Cashdollar, K.L. & Zlochower, I.A. (2000). Experimental mine and laboratory dust explosion research at NIOSH. *Journal of Loss Prevention in the Process Industries*, 13, pp. 229-242.
2. Lebecki, K., Sliz, J., Cybulski, K. & Dyduch, Z. (2001). Efficiency of triggered barriers in dust explosion suppression in galleries. *Journal of Loss Prevention in the Process Industries*, 14, pp. 489-494.
3. Grumer, J. (1974). Resent research concerning extinguishment of coal dust explosions. *Fifteenth Symposium (Int.) on Combustion*, pp. 103-114.
4. Faraday, M. & Lyell, C. (1845). Report on the explosion at the Haswell Collieries, and on the means of preventing similar accidents. *Philosophical Magazine*, 26, pp. 16-35.
5. Eckhoff, R.K. (2003). *Dust explosions in the process industries*. 3rd ed., Amsterdam: Gulf Professional Publishing.
6. Cybulski, W. (1975). *Coal dust explosions and their suppression*. Foreign Publications Department of the National Center for Science, Technical and Economic Information (translated from Polish), Warsaw, Poland.
7. Richmond, J.K. & Liebman, I. (1974). A physical description of coal mine explosions. *Fifteenth Symposium (Int.) on Combustion*, pp. 115-126.
8. Cybulski, W.B. (1971). Detonation of coal dust. *Bulletin de L'Academie Polonaise des Sciences*, XIX (5), pp. 37-41.
9. DESC (2001). *Development of a CFD-code for prediction of the potential consequences of dust explosions in complex geometries – Contract no. GRD1-CT-2001-00664*. Fifth framework programme, program acronym: *GROWTH*; project no.: *GRD1-2001-40340*, project acronym: *DESC*.
10. Skjold, T. (2007). Review of the DESC project. *Journal of Loss Prevention in the Process Industries*, 20, pp. 291-302.
11. Kosinski, P., Hoffmann, A.C. & Klemens, R. (2005). Dust lifting behind shock waves: comparison of two modelling techniques. *Chemical Engineering Science*, 60, pp. 5219-5230.
12. Klemens, R., Zydak, P., Kaluzny, M., Litwin, D. & Wolanski, P. (2006). Dynamics of dust dispersion from the layer behind the propagating shock wave. *Journal of Loss Prevention in the Process Industries*, 9, pp. 200-209.
13. Zydak, P. & Klemens, R. (2007). Modelling of dust lifting process behind propagating shock wave. *Journal of Loss Prevention in the Process Industries*, 20, pp. 417-426.
14. Lebecki, K., Sliz, J., Dyduch, Z. & Cybulski, K. (1993). Course of grain dust explosions in tunnels. In [15], pp. 171-187.
15. Wolanski, P. (1993). *Grain dust explosion and control*. Final Report, Grant no. FG-Po-370, Project no. PL-ARS-135, Institute of Heat Engineering, Warsaw University of Technology, Warsaw.
16. Lebecki, K., Cybulski, K., Sliz, J., Dyduch, Z. & Wolanski, P. (1995). Large scale grain dust explosion-research in Poland. *Shock Waves*, 5, pp. 109-114.
17. Patankar, S.V. (1980). *Numerical heat transfer and fluid flow*. Taylor & Francis.
18. Lauder, B.E. & Spalding, D.P. (1974). The Numerical Computation of Turbulent Flows. *Computer Methods in Applied Mechanics and Engineering*, 3, 269-289.
19. Arntzen, B.J. (1998). *Modelling of turbulence and combustion for simulation of gas explosions in complex geometries*. Dr. Ing. Thesis, NTNU, Trondheim, Norway.

20. Bray, K.N.C. (1990). Studies of the turbulent burning velocity. *Proc. R. Soc. Lond. A*, 431, pp. 315-335.
21. Abdel-Gayed, R.G., Bradley, D. & Lawes, M. (1987). Turbulent burning velocities: A general correlation in terms of straining rates. *Proc. R. Soc. Lond. A*, 414, pp. 389-413.
22. Marble, F.E. (1970). Dynamics of dusty gases. *Ann. Rev. Fluid Mechanics*, 2, pp. 397-446.
23. Crowe, C., Sommerfeld, M & Tsuji, Y. (1998). *Multiphase flows with droplets and particles*. Boca Raton: CRC Press.
24. Klemens, R. (2002-2005). *Reports I-V* to the DESC project, dated 2002, July 2003, January 2004, June 2004, and January 2005, respectively. Warsaw University of Technology, Poland.
25. Skjold, T., Y.K. Pu, Arntzen, B.J., Hansen, O.J., Storvik, I.E., Taraldset, O.J. & Eckhoff, R.K. (2005). Simulating the influence of obstacles on accelerating dust and gas flames. Poster, *Twentieth International Colloquium of Dynamics of Explosions and Reactive Systems* (ICDERS), July 31 - August 5, Montreal, Canada.
26. Skjold, T. (2007). Simulating the effect of release of pressure and dust lifting on coal dust explosions. *Twenty-first International Colloquium of Dynamics of Explosions and Reactive Systems* (ICDERS), Poitiers, France, July 23-27, 2007.